

# Nanoparticles Loaded with Pralidoxime Wrapped in Tumor Cell Membranes: A New Strategy to Counteract the Central Nervous System Effects of Organophosphate Poisoning

Huaizhi Jiang<sup>1,2</sup>, Yanli Liu<sup>2</sup>, Chu Wang<sup>1,2</sup>, Yunyang Song<sup>2</sup>, Fanghui Wu<sup>2</sup>, Yifeng Yin<sup>2</sup>, Zhanjun Yang<sup>3</sup>

<sup>1</sup>Department of Human Anatomy, Baotou Medical College, Inner Mongolia, Baotou, 014040, People's Republic of China; <sup>2</sup>State Key Laboratory of NBC Protection for Civilian, Beijing, 102205, People's Republic of China; <sup>3</sup>Department of Human Anatomy, Chifeng University, Inner Mongolia, Chifeng, 024000, People's Republic of China

Correspondence: Zhanjun Yang; Yifeng Yin, Email yzj8330@163.com; 13683534354@163.com

**Purpose:** In this study, cell membrane-coated nanoparticles (CMCNPs) were loaded with the organophosphorus antidote Pralidoxime Chloride (PAM) to improve the ability of the drug to penetrate the blood–brain barrier (BBB) and evade immune clearance, providing a novel drug delivery strategy for the treatment of central organophosphorus poisoning.

**Methods:** 1) The cell membranes of mouse melanoma cells (B16F10), breast cancer cells (4T1), glioblastoma cells (GL261), and monocytic macrophage leukemia cells (RAW264.7) were extracted, and their purities were verified. The cell membranes were combined with PAM in mesoporous silica (SiO<sub>2</sub>) spheres by ultrasonic fusion to prepare the CMCNPs. 2) The immune evasion ability of CMCNPs was evaluated by laser confocal microscopy and flow cytometry after coculture with macrophages. 3) HPLC was used to screen the best CMCNPs through an in vitro BBB model. 4) After the CMCNPs were injected into malathion-poisoned mice, the phosphate chloride concentration in the peripheral blood and brain homogenates was tested, and the rate of acetylcholinesterase (AChE) reactivation was determined.

**Results:** All four types of CMCNPs were spherical particles with diameters of approximately 100 nm. Compared with unwrapped nanoparticles, CMCNPs exhibited a stronger immune evasion ability and enhanced BBB penetration ability in an in vitro BBB model. They also significantly prolonged the in vivo circulation time of PAM, increased its delivery dose to the central nervous system, and markedly increased cholinesterase activity in brain tissues. Furthermore, in an organophosphorus-poisoned mouse model, CMCNPs significantly improved the survival rate of intoxicated mice.

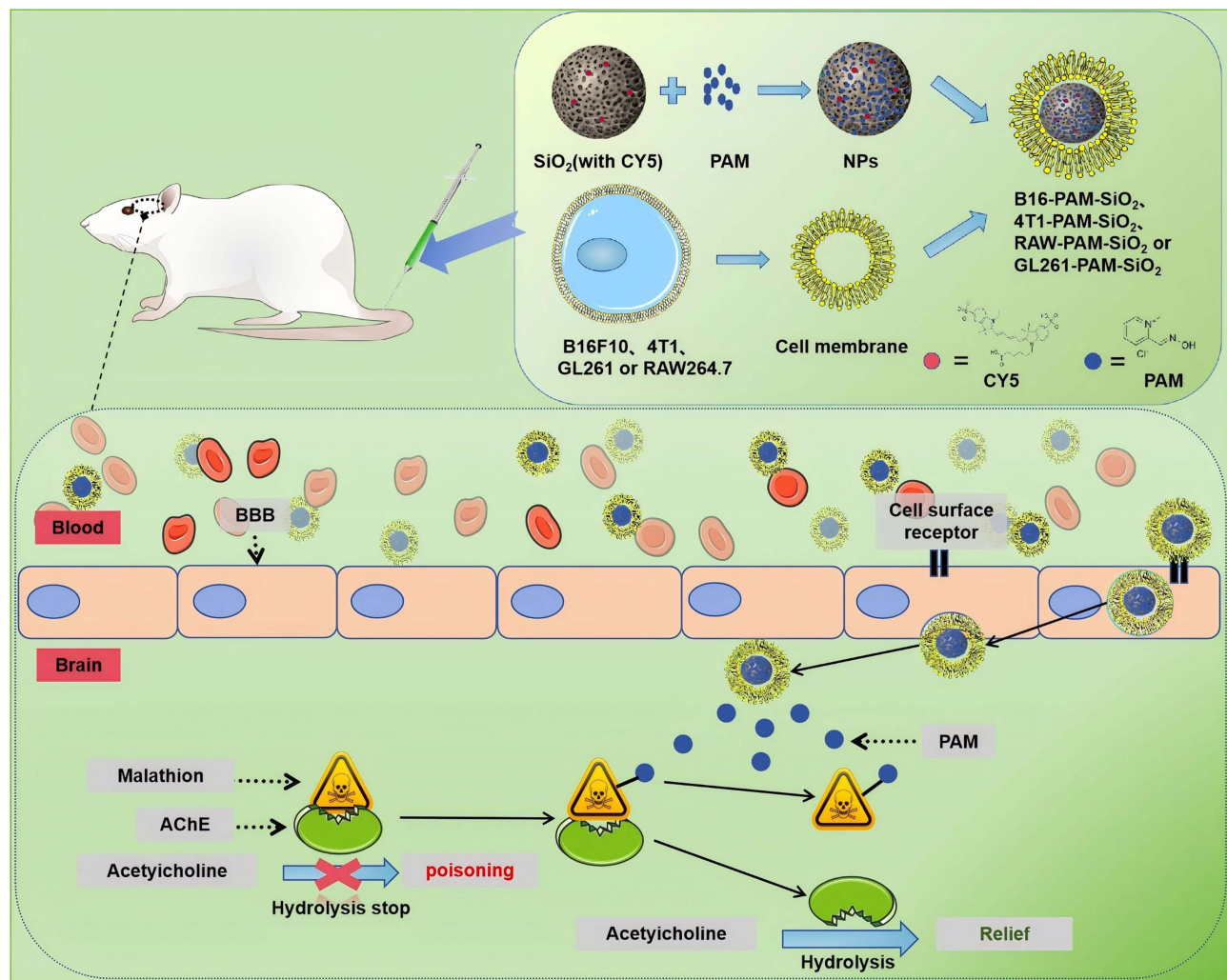
**Conclusion:** In this study, CMCNPs with a significant BBB penetration ability and immune evasion ability were successfully prepared and improved the therapeutic effect of PAM on central organophosphate poisoning.

**Keywords:** cell membrane wrapping, nanoparticles, blood–brain barrier, organophosphorus poisoning, pralidoxime chloride

## Introduction

Organophosphate (OP) compounds represent a double-edged sword in modern agriculture.<sup>1</sup> Their low production cost and high insecticidal efficacy have led to their widespread global use, with organophosphorus pesticides constituting more than 38% of total pesticide consumption.<sup>2</sup> However, acute poisoning caused by accidental exposure or intentional misuse remains a critical public health challenge. Annually, approximately 3 million OP poisoning cases are reported worldwide, resulting in 200,000 fatalities, underscoring the urgent need for improved therapeutic interventions.<sup>3,4</sup> The primary toxicity mechanism involves the irreversible inhibition of acetylcholinesterase (AChE), leading to excessive cholinergic signaling and life-threatening neurological symptoms.<sup>5,6</sup> Current treatments, such as oxime reactivators (eg, pralidoxime),<sup>7</sup> are limited by poor blood–brain barrier (BBB) penetration, and central nervous system (CNS) toxicity is inadequately addressed.

## Graphical Abstract



Nearly 98% of small-molecule drugs and the vast majority of large-molecule therapeutics are incapable of crossing the intact BBB under physiological conditions.<sup>8–10</sup> Researchers have turned their attention to nanoparticle-based drug delivery systems to address this limitation. These systems combine drug-loaded nanoparticle cores (including gold, silver, carbon dots, and organic polymers)<sup>11–13</sup> with diverse surface modification techniques (such as PEGylation<sup>14</sup> and transferrin conjugation<sup>15</sup>) through flexible combinations to achieve the desired delivery objectives, particularly CNS-targeted delivery.<sup>8</sup> However, conventional polymeric nanoparticles face challenges such as rapid immune clearance (eg, by the reticuloendothelial system) and batch-to-batch variability in size or surface charge, which may promote unintended interactions with immune cells and trigger inflammatory responses.<sup>8,10</sup>

Emerging as a breakthrough in nanomedicine, cell membrane-coated nanoparticles (CMCNPs) integrate drug-loaded cores with natural membrane shells (eg, erythrocyte or cancer cell membranes). This biomimetic design not only exhibits enhanced biocompatibility but also enables tissue-specific homing, addressing critical challenges in traditional nanoparticle therapies. Recent studies highlight their potential in overcoming biological barriers for CNS drug delivery, positioning CMCNPs as a transformative platform for next-generation precision medicine.<sup>16–18</sup> Biomimetic nanocomposites can mimic the properties of source cells with a wide range of desirable functions, such as prolonged cycle times and disease-associated targeting.<sup>8</sup> According to Wang et al, fluorescently labeled nanoparticles with brain metastasis-

capable tumor cell membranes can penetrate the BBB to target tumor cells during brain metastasis. Compared with naked nanoparticles, the constructed CMCNPs significantly improved blood–brain barrier penetration and immune escape.<sup>19</sup> Macrophage membrane-coated solid lipid nanoparticles inherit the immune characteristics of macrophages and prevent the nanoparticles from being captured by the reticular endothelial system. A biomimetic nanoformulation can effectively cross the BBB to target neuronal cells and further localize to the mitochondria to inhibit the production of reactive oxygen species, protect neurons, inhibit their apoptosis, and effectively delay the progression of Alzheimer’s disease.<sup>20</sup> Liu et al reported that the use of a glioma cell membrane to deliver treatment to brain tumors prolonged the blood circulation time of the drug, improved the BBB permeability and increased drug accumulation and retention in drug-resistant tumors.<sup>21</sup> In conclusion, CMCNPs have unique advantages over other approaches in targeting drug delivery to the CNS.

To date, no previous attempts to utilize CMCNPs to counteract OP poisoning have been reported. This study aimed to develop a biomimetic nanocarrier with a core–shell structure for the targeted treatment of central nervous system OP poisoning. The core consists of mesoporous silica nanoparticles labeled with CY5 fluorescence, enabling dual functionality for drug loading and real-time imaging. The shell was engineered using tumor cell membranes derived from four distinct cancer cell lines: B16F10 melanoma, 4T1 breast carcinoma, GL261 glioblastoma, and RAW264.7 macrophage leukemia cells. These membranes were selected based on their documented roles in BBB penetration (GL261), immune evasion (RAW264.7), and brain tropism (B16F10/4T1). We hypothesize that the hybrid membrane coating synergistically confers BBB traversal, immune escape, and brain-targeted delivery capabilities to the nanocarrier, thereby increasing the efficacy of OP antidotes in the CNS.

## Materials and Methods

### Materials

Mesoporous silica nanospheres (approximately 80 nm in diameter) fluorescently labeled with CY5 were purchased from Xi’an Ruixi Biotechnology Co., Ltd. (Xi’an, China). Malathion (O, O-dimethyl-S-(1,2-dicarbethoxyethyl) dithiophosphate) at 95% purity was purchased from Dezhou Green Ba Fine Chemical Co., Ltd. (Dezhou, Shandong, China). Pralidoxime Chloride (93% purity) was obtained from the State Key Laboratory of National Nuclear and Biochemical Disaster Prevention (Beijing, China), and the chlorophospidine standard was purchased from the China Institute for Food and Drug Control (Beijing, China). The BCA protein quantitative analysis kit, acetonitrile, sodium n-heptane sulfonate, and trifluoroacetic acid were purchased from Thermo Fisher Scientific (Waltham, MA, USA). The acetylcholinesterase (AChE) activity detection kit was purchased from BioEngineering Co., Ltd. (Shanghai, China). Tris-HCl, D-mannitol, sucrose, EGTA, and polyacrylamide (4% to 15%) for denaturing gel electrophoresis were purchased from Solebio (Beijing, China).

### Animals and Cells

#### Animals

A total of 150 male Kunming white mice, aged 10 weeks and weighing 30±2 g, were purchased from Beijing Huafukang Biotechnology Co., Ltd. (License No. SCXK (Jing) 2019–0008). The experimental animals were housed at room temperature 22±1 °C with a 12-hour light/dark cycle and had free access to food and water. The care and use of experimental animals followed the “3R” principles and the “Guide for the Care and Use of Laboratory Animals” in China.

#### Cells

Murine melanoma cells (B16F10), breast cancer cells (4T1), mouse glioblastoma cells (GL261), mouse monocyte macrophage leukemia cells (RAW264.7), and immortalized human brain microvascular endothelial cells (hCMEC/D3) were purchased from Anwei Biotechnology Co., Ltd. (Shanghai, China).

### Preparation of Cell Membrane-Coated Nanoparticles

The four cancer cell lines, mouse melanoma cells (B16F10), mouse glioblastoma cells (GL261), mouse monocyte macrophage leukemia cells (RAW264.7), and mouse breast cancer cells (4T1), were cultured in media containing 10% fetal calf serum and

1% antibiotics (100 U/mL penicillin and 100 µg/mL streptomycin). The basal medium used for B16F10 cells was DMEM (Gibco), and the basal medium for GL261 cells was DMEM supplemented with 2 mm L-glutamine (Gibco). The basal medium used for RAW264.7 cells was DMEM (Gibco) supplemented with 2 mm L-glutamine and 0.11 g/L sodium pyruvate. The basal medium used for the 4T1 cells was RPMI 1640 (Gibco). All four cell lines were cultured at 37 °C with 5% CO<sub>2</sub> and monitored under a microscope. After reaching a growth density of 70% to 80%, the cells were washed three times with PBS (HyClone), suspended in a hypotonic solution (225 mm D-mannitol, 30 mm Tris-HCl, 0.2 mm EGTA and 75 mm sucrose), and then centrifuged at 20000 × g for 25 min at 4 °C. The supernatant was transferred to a new centrifuge tube and centrifuged again for 35 min at 100,000 × g and 4 °C. After centrifugation, the supernatant was discarded, and the precipitate contained the cell membranes. After the protein content of the membrane was measured via a BCA kit, the samples were stored at -80 °C in the short term. CY5-labeled mesoporous silica nanospheres (3 mg) were mixed with pralidoxime chloride (PAM, 15 mg) in 7.5 mL of PBS (pH 7.4). The mixture was stirred at 400 rpm for 8 hours using a magnetic stirrer (IKA RCT Basic, 4 °C) to allow the PAM to adsorb to mesoporous silica, forming nanosilica nanospheres (hereafter named PAM-SiO<sub>2</sub>). Finally, the PAM-SiO<sub>2</sub> solution (0.5 mL, the concentration of PAM was 2 mg/mL) and the cell membrane solution (0.5 mL, with a protein-adjusted concentration of 2 mg/mL) were mixed and sonicated using a probe sonicator (SCIENTZ - IID, 20% amplitude, 5 second pulse-on/10 second pulse-off) for 3 min on ice to obtain the four CMCNPs (B16-PAM-SiO<sub>2</sub>, 4T1-PAM-SiO<sub>2</sub>, RAW-PAM-SiO<sub>2</sub>, and GL261-PAM-SiO<sub>2</sub>). After preparation, the samples were stored at 4 °C for a short period.

## Morphology and Characterization of the Cell Membrane-Coated Nanoparticles

The above prepared biomimetic nanoparticles (B16-PAM-SiO<sub>2</sub>, 4T1-PAM-SiO<sub>2</sub>, RAW-PAM-SiO<sub>2</sub> and GL261-PAM-SiO<sub>2</sub>) were negatively stained according to methods described in the literature,<sup>22</sup> and successful fusion of the cell membrane and PAM-SiO<sub>2</sub> nanoparticles was verified by transmission electron microscopy (TEM).

### Characterization of Cell Membrane-Coated Nanoparticles

The particle size distribution was measured by electron microscopy imaging and the software Nano Measurer 1.2. The zeta potential of the nanoparticles was measured using a Zetasizer Nano ZS (Malvern Instruments Ltd., UK).

### Determination of the Encapsulation Efficiency of the Nanoparticles

The encapsulation efficiency was determined by placing the four nanoparticle solutions with a PAM concentration of 3 mg/mL in 100 kDa ultrafiltration tubes, centrifuging them at 4000 × g for 30 min to remove the free drug, washing the nanoparticles twice with 40 times the volume of ultrapure water, combining the filtrates, and measuring the free drug content (F) by HPLC.

The specific parameters of the HPLC method were as follows: CAPCELL PAKC18MG III (250 mm×4.6 mm, 5 µm) chromatographic column; column temperature, 30 °C; mobile phase A, 5 mmol/L sodium heptane sulfonate containing a volume ratio of 0.12% trifluoroacetic acid; phase B, acetonitrile; flow rate, 1 mL/min; detection wavelength, 294 nm; sample intake, 20 µL; and gradient elution (0–5 min, 92% A; 5–15 min, 92% A→80% A; 15–25 min, 80% A; and 25–35 min, 80% A→92% A).

The encapsulation efficiency of the CMCNPs was calculated using the following equation:

$$\text{Encapsulation efficiency(\%)} = \frac{T - F}{T} \times 100\%$$

where T is the total drug volume input (mg) and F is the amount of free drug (mg) not encapsulated in the nanoparticles.

### Drug Release from the Nanoparticles in vitro

One milliliter of CMCNPs solution containing 5 mg/mL PAM was added to the dialysis bag (MWCO 3000), both ends of the dialysis bag were sealed, the dialysis bag was placed in a 50 mL centrifuge tube, and 25 mL of PBS (pH=7.4) solution was added to the centrifuge tube. The centrifuge tube was shaken at 37 °C and 100 rpm. At 0.5 h, 1 h, 2 h, 3 h, 3 h, 4 h, 6 h, 8 h, 12 h, and 24 h, 1 mL of solution was removed, and 1 mL of PBS solution was added to the centrifuge tube. A release curve was drawn for the PAM drug content measured using HPLC. The specific parameters of the HPLC method were as follows: CAPCELL PAKC18MG III (250 mm×4.6 mm, 5 µm) chromatography column; column temperature, 30 °C; mobile phase A, 5 mmol/L

sodium heptane sulfonate containing 0.12% trifluoroacetic acid by volume; phase B, acetonitrile; flow rate, 1 mL/min; detection wavelength, 294 nm; sample intake, 20  $\mu$ L; and gradient elution (0–5 min, 92% A; 5–15 min, 92% A→80% A; 15–25 min, 80% A; and 25–35 min, 80% A→92% A).

## In vitro BBB Model Construction

### Construction and Evaluation of the in vitro BBB Model

An in vitro BBB was first constructed and evaluated before testing to assess whether nanocarriers covered by metastatic cancer cell membranes could cross the BBB in vitro. First,  $1 \times 10^4$  hCMEC/D3 cells were seeded into 1% polylysine-coated 24-well Transwell plates and cultured in DMEM supplemented with 5% FBS, 1% antibiotics (100 U/mL and 100 U/mL and 100  $\mu$ g/mL streptomycin) and 1% endothelial cell culture additive at 37 °C with 5% CO<sub>2</sub>. The solution was changed daily, and cell growth was observed under an inverted microscope. Transmembrane resistance measurements and fluorescein sodium permeability experiments were performed on the model for approximately 2–3 days.

### Measurement of Transendothelial Electrical Resistance

Transendothelial resistance (TEER) was tested to quickly and easily determine the integrity and function of tight junctions in a single-cell culture model of endothelial cells. The transendothelial resistance values of the models were measured using a Millicell<sup>®</sup> ERS-2 instrument. The electrode was inserted vertically into the Transwell chamber, the short electrode was placed in the upper chamber, the long electrode was placed in the lower chamber, the electrode piece was inserted below the liquid level, and the displayed resistance value ( $\Omega$ ) was recorded.

$$\text{Valid resistance value } (\Omega \cdot \text{cm}^2) = (A_C - A_0) \times S$$

where  $A_C$  is the resistance value of wells containing cells ( $\Omega$ );  $A_0$  is the resistance value of the blank wells ( $\Omega$ ); and  $S$  is the membrane area ( $\text{cm}^2$ ).

### Fluorescein Sodium Permeability Test

The maximum absorption peak intensity of fluorescein sodium (FLU) at concentrations of 0, 0.1, 1, 10 and 100  $\mu$ g/mL was determined using a microplate reader, with four complex wells for each sample, and a standard curve was drawn. FLU penetration into the hCMEC/D cell monolayer was determined according to established methods.<sup>23,24</sup> (1) In the hCMEC/D alone culture group and Transwell blank control group (no cells were added), the upper and lower chambers were cleaned with D-Hank's buffer before determination. (2) A total of 1 mL of 100  $\mu$ g/mL FLU was added to the upper chamber, 2 mL of D-Hank's buffer was added to the lower chamber, and the mixture was incubated for 60 min before 500  $\mu$ L of liquid was collected from the lower chamber. (3) The collected samples were diluted and added to 96-well plates to determine the fluorescence value (excitation wavelength of 490 nm and emission wavelength of 515 nm), and the amount of FLU penetration in the model group and the blank control group was calculated according to the FLU standard curve. (4) The permeability coefficient of FLU was calculated as follows to evaluate the permeability of the BBB model:

$$\text{Removed volume : } V_R(\text{mL}) = \frac{C_A \times V_A}{C_I}$$

$$\text{Clearance : } A(\text{mL} \cdot \text{min}^{-1}) = \frac{V_R(\text{mL})}{T(\text{min})}$$

$$\text{Permeability coefficient : } P = A/S$$

$$P_{sc} = P_{sf} \times P_{st} / (P_{sf} - P_{st})$$

where  $C_A$  is the liquid concentration in the lower chamber;  $V_A$  is the liquid volume in the lower chamber;  $C_I$  is the initial liquid concentration in the upper chamber;  $P_{st}$  is the permeability surface area of the model group;  $P_{sf}$  is the permeability surface area of the blank group; and  $S$  is the membrane area of the cell culture pool. For this experiment,  $S$  is 0.33  $\text{cm}^2$ .

## In vitro BBB Model Testing

### Cytotoxicity of the Nanoparticles to hCMEC/D3 Cells

The cytotoxicity of the nanoparticles to hCMEC/D3 cells was measured via a CCK-8 assay. First, the cells ( $1 \times 10^4$  cells/well) were seeded in 96-well plates and cultured for 24 h. After hCMEC/D3 cells, the main component of the blood–brain barrier, were cultured with different concentrations of SiO<sub>2</sub> (0.5, 1, 2, 4, 8, and 16 μg/mL) of PAM-SiO<sub>2</sub>, B16-PAM-SiO<sub>2</sub>, 4T1-PAM-SiO<sub>2</sub>, RAW-PAM-SiO<sub>2</sub>, and GL261-PAM-SiO<sub>2</sub> for 8 h, 10 μL of CCK-8 solution was added to each well, incubated again in the incubator for 2 h, and the OD at 450 nm was measured with a microplate reader. Cell viability was calculated according to the following formula to determine acceptable experimental concentrations that do not affect cell activity:

$$\text{Cell viability(\%)} = \frac{A_{\text{sample}} - A_0}{A_{\text{control}} - A_0} \times 100\%$$

$A_{\text{sample}}$  is the OD of wells with cells, CCK-8 solutions, and nanoparticles;

$A_0$  is the OD of wells with medium and CCK-8 solution without cells; and

$A_{\text{control}}$  is the OD of wells with cells and CCK-8 solution without nanoparticles.

### In vitro BBB Permeability of the Nanoparticles

SiO<sub>2</sub> at a concentration of 16 μg/mL in the form of PAM-SiO<sub>2</sub>, B16-PAM-SiO<sub>2</sub>, 4T1-PAM-SiO<sub>2</sub>, RAW-PAM-SiO<sub>2</sub>, or GL261-PAM-SiO<sub>2</sub> was added to the upper chamber of a successfully constructed BBB to evaluate whether nanocarriers coated with cancer cell membranes could cross the BBB in vitro. The solution in the lower chamber was collected to measure the fluorescence intensity, and the concentration of pralidoxime chloride was detected using high-performance liquid chromatography.

A BBB model with an effective resistance value greater than  $50 \Omega \cdot \text{cm}^2$  was selected. The 24-well Transwell plates were washed with D-Hank's buffer. Five groups were prepared. PAM-SiO<sub>2</sub>, B16-PAM-SiO<sub>2</sub>, 4T1-PAM-SiO<sub>2</sub>, RAW-PAM-SiO<sub>2</sub> or GL261-PAM-SiO<sub>2</sub> were mixed with D-Hank's solution at 16 μg/mL, 0.6 mL was added to the upper chamber of the 6-well Transwell plate, and 1.5 mL of D-Hank's buffer was added. The fluid from the lower chamber was collected 8 h later.

First, fluorescence measurements were performed. With the CY5 fluorescence label on the surface, the number of silicon nanoparticles penetrating the external BBB was laterally verified by measuring the CY5 fluorescence intensity in the lower chamber (excitation wavelength: 640 nm; emission wavelength: 680 nm). After the sample was fully sonicated (30% for 3 min), it was centrifuged (15000 rpm, 20 min) to elute the phosphorus from the mesoporous silica nanoparticles. After ultrafiltration (with a 100 kDa ultrafiltration column), the filtrate was removed to determine the concentration of phosphorus in the sample filtrate.

### Nanoparticle Immune Escape Experiments

The cell membrane wrapped around the nanoparticle surface can inherit many of the interface features of the original cell, such as the immune escape ability. RAW264.7 macrophages were seeded in dishes ( $1 \times 10^5$  cells) and cultured for 24 h. The cells were then incubated for 8 h with PAM-SiO<sub>2</sub>, B16-PAM-SiO<sub>2</sub>, 4T1-PAM-SiO<sub>2</sub> or GL261-PAM-SiO<sub>2</sub>. After three washes with PBS, the nuclei were stained with DAPI at 37 °C for 15 min, and the cells were analyzed by confocal laser scanning microscopy and flow cytometry. Nanoparticles with a strong immune escape ability are not easily captured by macrophages and are washed away in the washing step. Thus, the more the nanoparticles bound to the cells, the stronger the fluorescence became, indicating a weaker immune escape capability.

## In vivo Experiment

Based on the results of the in vitro tests (see the Results: In vitro model testing) regarding BBB penetration and immune escape, the ability of the naked PAM-SiO<sub>2</sub> nanoparticles to cross the mouse BBB was tested in vivo. The mice were injected with PAM-SiO<sub>2</sub> and two biomimetic nanoparticles at a SiO<sub>2</sub> dose of  $0.3 \text{ mg} \cdot \text{kg}^{-1}$  via the tail vein. Because the silicon nanoparticle itself carries a CY5 fluorescent label, the distribution of the drug can be determined using a live fluorescence imaging system. PAM, PAM-SiO<sub>2</sub>, B16-PAM-SiO<sub>2</sub>, and GL261-PAM-SiO<sub>2</sub> were injected, and the

concentrations of phosphoridine in the serum and brain homogenates were measured by high-performance liquid chromatography. The activity in the serum and brain homogenates was determined using the Ellman method.

### In vivo Fluorescence Imaging Analysis

Mice were injected with 1.5 mg/kg PAM in the form of vehicle containing PAM-SiO<sub>2</sub>, B16-PAM-SiO<sub>2</sub>, or GL261-PAM-SiO<sub>2</sub> via the tail vein. Fluorescence imaging of live animals was performed using a fluorescent animal imaging system with an excitation wavelength of 640 nm and an emission wavelength of 680 nm. The distribution of fluorescence in the mice, especially in the brain, was examined at 0, 1, 2, 4, 8, 12 and 24 h after injection. After 24 hours of imaging, intact brain tissue from the mice was removed on ice, and the fluorescence intensity in the mouse brain was measured again.

### Pharmacokinetic and Pharmacodynamic Experiments

Thirty Kunming mice were randomly divided into 6 groups (5 mice per group): Group 1 was the blank control group, and the mice in Groups 2 to 6 were subcutaneously injected with 1.25 g/kg malathion. One hour later, the mice in Group 2 were injected with normal saline via the tail vein, while the mice in Groups 3, 4, 5, and 6 were injected with 22.5 mg/kg (1/4LD50) PAM in the form of pralidoxime chloride, PAM-SiO<sub>2</sub>, B16-PAM-SiO<sub>2</sub>, and GL261-PAM-SiO<sub>2</sub>, respectively. Four hours later, 1 mL of blood was collected from the heart and centrifuged twice at 4 °C and 5000 rpm for 20 min to extract the serum; the brain tissue was removed on ice after decapitation, mechanically ground, homogenized at -4 °C for 3 min, and then centrifuged at 12000 rpm and 4 °C for 5 min, after which the supernatant was collected for further use. The concentrations of PAM in the serum and brain homogenate supernatants were measured by high-performance liquid chromatography. The activity of AChE in the serum and brain homogenate supernatants was determined using the Ellman method. The principle of the Ellman method is as follows: AChE catalyzes the hydrolysis of acetylcholine (ACh) to produce choline, which reacts with 5,5'-dithiobis-(2-nitrobenzoic acid) (DTNB) to form 5-thio-2-nitrobenzoic acid (TNB). TNB has an absorption peak at 412 nm, and the activity of the AChE enzyme can be determined by measuring the rate of increase in the absorbance (OD) at 412 nm. The formula for calculating the AChE reactivation rate (RR) is as follows:

$$RR\% = \frac{OD[\text{group}_n] - OD[\text{group}_2]}{OD[\text{group}_1] - OD[\text{group}_2]} \times 100\% \quad n : 3, 4, 5 \text{ and } 6.$$

The concentration of pralidoxime chloride, the activity of AChE, and the reactivation rate of AChE in the mice were determined at 12 hours and 24 hours using the same method.

### CMCNPs Treatment for Malathion Poisoning

An analysis of the overall survival rate of the animals was conducted to further clarify the advantages of CMCNPs in rescuing mice from malathion poisoning. Fifty Kunming mice were randomly divided into five groups of 10 mice each. A subcutaneous injection of 1.25 g/kg malathion was administered to Kunming mice. One hour later, saline or PAM, PAM-SiO<sub>2</sub>, B16-PAM-SiO<sub>2</sub>, or GL261-PAM-SiO<sub>2</sub> containing 22.5 mg/kg (1/4LD50) pralidoxime chloride was injected into the tail veins of the mice in the different groups. The survival status of the five groups of mice was recorded at three time points: 4 hours, 12 hours, and 24 hours.

## Results

We integrated key methodologies and their outcomes to systematically evaluate the synthesis and characteristics of cell membrane-coated nanoparticles, as shown in [Table 1](#).

### Morphology and Characterization of CMCNPs

We first determined whether the cell membranes were successfully fused with PAM-SiO<sub>2</sub> nanoparticles by measuring the zeta potential of the nanoparticles (PAM-SiO<sub>2</sub>, B16-PAM-SiO<sub>2</sub>, 4T1-PAM-SiO<sub>2</sub>, RAW-PAM-SiO<sub>2</sub>, and GL261-PAM-SiO<sub>2</sub>) using a Zetasizer Nano, followed by observing their morphology and size via transmission electron microscopy (TEM) with negative staining. The TEM results revealed that the synthesized CMCNPs consisted of a core of PAM-SiO<sub>2</sub> and an outer layer of a cell membrane wrapper ([Figure 1A–E](#)). The diameter of the unwrapped PAM-SiO<sub>2</sub> particles was

**Table 1** Summary of the Key Results

Research Content	Key Methods	Summary of Results
CMCNPs Construction	<ul style="list-style-type: none"> <li>• Tumor membrane extraction (centrifugation)</li> <li>• PAM loading (electrostatic adsorption)</li> <li>• Ultrasonic fusion</li> </ul>	<ul style="list-style-type: none"> <li>• Four CMCNPs were synthesized: B16-, 4T1-, RAW-, and GL261-PAM-SiO<sub>2</sub>.</li> </ul>
CMCNPs Characterization	<ul style="list-style-type: none"> <li>• TEM imaging</li> <li>• Zeta potential measurements</li> <li>• Encapsulation efficiency tests</li> <li>• Release kinetic experiments</li> </ul>	<ul style="list-style-type: none"> <li>• The core-shell structure was confirmed</li> <li>• Zeta ↓10 mV</li> <li>• 80% encapsulation</li> <li>• The release rate was slightly lower than uncoated PAM-SiO<sub>2</sub></li> </ul>
In Vitro Testing (four particles)	<ul style="list-style-type: none"> <li>• hCMEC/D3 Transwell model</li> <li>• Immune evasion (macrophage uptake)</li> </ul>	<ul style="list-style-type: none"> <li>• 2.8× higher BBB penetration compared with uncoated NPs</li> <li>• 2.4× reduced phagocytosis</li> <li>• Ranking: GL261 &gt; B16 &gt; RAW &gt; 4T1</li> </ul>
B16-PAM-SiO <sub>2</sub> and GL261-PAM-SiO <sub>2</sub> with optimal BBB penetration and immune evasion capability were selected for in vivo testing.		
In Vivo Testing (two particles)	<ul style="list-style-type: none"> <li>• Fluorescence imaging</li> <li>• AChE activity assay</li> <li>• 24-h survival tracking</li> </ul>	<ul style="list-style-type: none"> <li>• 3.5× brain accumulation (B16-PAM-SiO<sub>2</sub>)</li> <li>• AChE activity was high in the CNS (CMCNPs vs PAM-SiO<sub>2</sub> and PAM)</li> <li>• 100% survival (CMCNPs vs the 50% control)</li> </ul>

75.23±7.47 nm, whereas the diameter of the nanoparticles wrapped by the cell membrane was significantly increased by 10–15 nm (Figure 1F). The zeta potential analysis indicated successful cell membrane encapsulation, with B16-PAM-SiO<sub>2</sub>, 4T1-PAM-SiO<sub>2</sub>, RAW-PAM-SiO<sub>2</sub>, and GL261-PAM-SiO<sub>2</sub> nanoparticles exhibiting a significant reduction of 10 mV compared with uncoated PAM-SiO<sub>2</sub> controls (Figure 1G). We placed the nanoparticles (B16-PAM-SiO<sub>2</sub>, 4T1-PAM-SiO<sub>2</sub>, RAW-PAM-SiO<sub>2</sub> and GL261-PAM-SiO<sub>2</sub>) in an ultrafiltration tube, collected the filtrate, and measured the free PAM in the filtrate by HPLC to detect the encapsulation of PAM in CMCNPs. The results revealed that the encapsulation efficiency of the CMCNPs was approximately 80% (Figure 1H). We added 1 mL of the CMCNPs solution to a dialysis bag (MWCO 3000) to determine whether the nanoparticles would affect PAM release, and the results revealed that the nanoparticles slowed the PAM release rate (Figure 1I).

## In vitro Model Testing

Five nanoparticles, PAM-SiO<sub>2</sub>, B16-PAM-SiO<sub>2</sub>, 4T1-PAM-SiO<sub>2</sub>, RAW-PAM-SiO<sub>2</sub> and GL261-PAM-SiO<sub>2</sub>, were placed in the upper chamber of an in vitro model to determine the penetration of each group and evaluate whether tumor cell membrane-covered nanoparticles could cross the blood-brain barrier in vitro. The key to this experiment was to first construct the BBB and evaluate whether the constructed BBB was accurate. In vitro BBB construction was performed by seeding  $1 \times 10^4$  hCMEC/D3 cells into 1% polylysine-coated 24-well Transwell plates. The solution was changed daily, and cell growth was observed under an inverted microscope. Fluorescein sodium permeability and transmembrane resistance were measured after cell fusion. (1) TEER monitoring of the hCMEC/D3 monolayer culture model was performed. At an inoculation density of  $1 \times 10^5$  cells/well, the TEER reached  $62.37 \Omega \cdot \text{cm}^2$  at 1–2 days of culture and peaked at  $102.63 \Omega \cdot \text{cm}^2$  at 5–6 days of culture. According to the literature,<sup>25,26</sup> in an in vitro BBB model constructed with hCMEC/D3 cells, when the TEER value exceeds  $50 \Omega \cdot \text{cm}^2$ , the cell layer grows densely and forms a barrier (Figure 2A). (2) A fluorescein sodium permeability experiment was subsequently performed. The permeability coefficient of FLU penetrating the in vitro BBB model at 60 min was  $0.33 \pm 0.04 \times 10^{-3} \text{ cm} \cdot \text{min}^{-1}$ , which is close to the reported range of  $0.34 \pm 0.14 \times 10^{-3} \text{ cm} \cdot \text{min}^{-1}$ .<sup>27</sup> These findings indicate that the established in vitro BBB model has low permeability, indicating successful model establishment. After successful establishment of the BBB in vitro, the permeability rate of the nanoparticles was determined. Before the development of the experiment, the cytotoxicity of different concentrations of PAM-SiO<sub>2</sub>, B16-PAM-SiO<sub>2</sub>, 4T1-PAM-SiO<sub>2</sub>, RAW-PAM-SiO<sub>2</sub> and GL261-PAM-SiO<sub>2</sub> toward hCMEC/D3 cells, the main components of the BBB, was tested to determine the optimal concentration. The results showed that at a SiO<sub>2</sub> concentration of 16 µg/mL (Figure 2B), these nanoparticles caused no significant cytotoxicity, indicating that this concentration can be used to determine the penetration rate of the nanoparticles through the BBB in vitro.

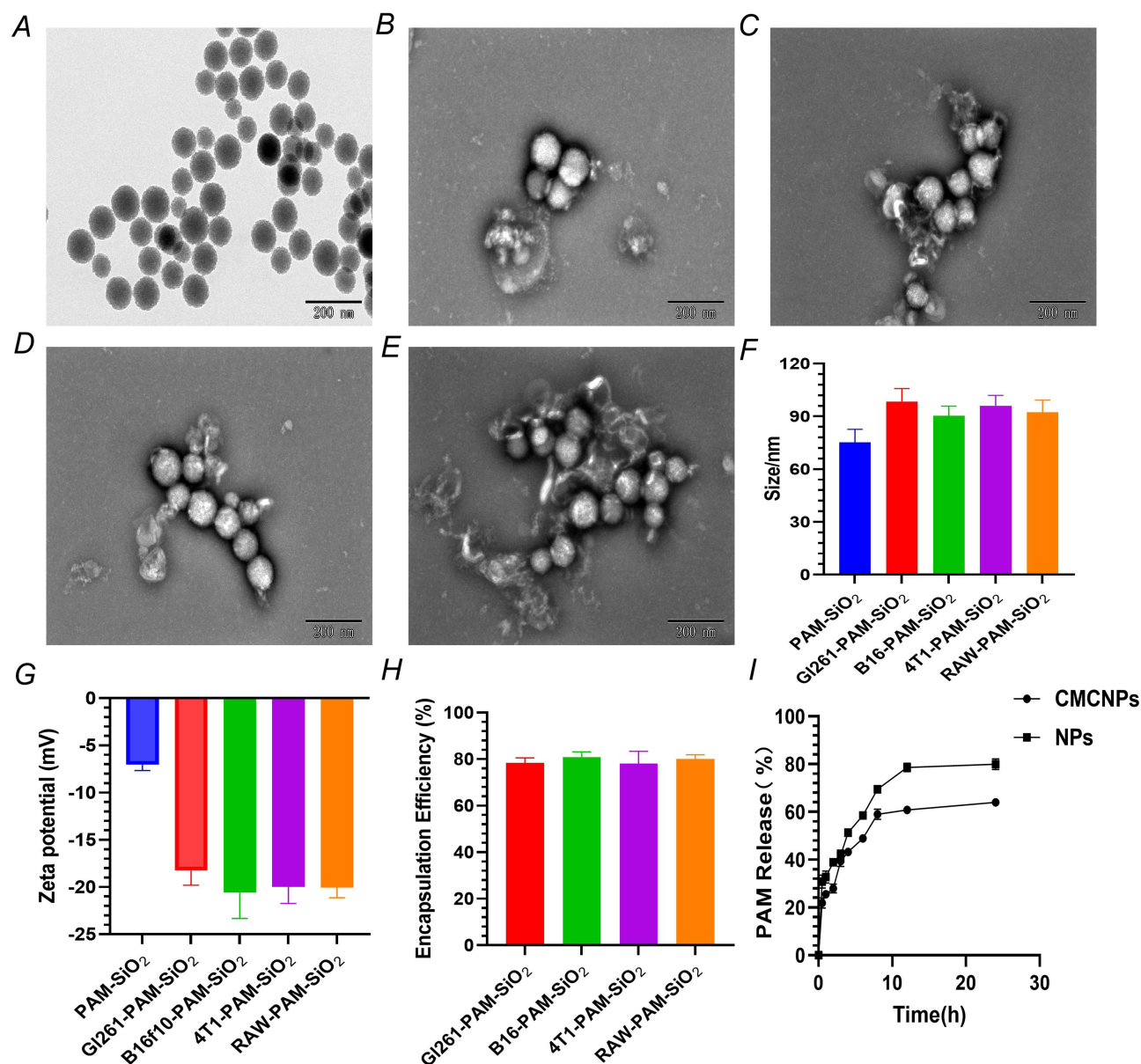


**Figure 1** Characterization of CMCNPs. (A-E) TEM images of PAM-SiO<sub>2</sub>, GI261-PAM-SiO<sub>2</sub>, B16-PAM-SiO<sub>2</sub>, 4T1-PAM-SiO<sub>2</sub>, and RAW-PAM-SiO<sub>2</sub>, with a scale bar of 200 nm. (F) Particle sizes of the five nanoparticles under an electron microscope: the PAM-SiO<sub>2</sub> diameter was 75.23±7.47 nm (n=10, the same as below); the GI261-PAM-SiO<sub>2</sub> diameter was 98.45±7.37 nm; the B16-PAM-SiO<sub>2</sub> diameter was 90.31±5.53 nm; the 4T1-PAM-SiO<sub>2</sub> diameter was 92.35±6.94 nm; and the RAW-PAM-SiO<sub>2</sub> diameter was 96.02±5.91 nm. (G) Zeta potential of PAM-SiO<sub>2</sub>, GI261-PAM-SiO<sub>2</sub>, B16-PAM-SiO<sub>2</sub>, 4T1-PAM-SiO<sub>2</sub>, and RAW-PAM-SiO<sub>2</sub> (n=6). (H) The encapsulation efficiency of the CMCNPs in each group. (I) In vitro release profiles of CMCNPs and NPs in PBS (n=3).

Each group of nanoparticles was added to the upper Transwell chamber at a final concentration of 16 μg/mL SiO<sub>2</sub> to assess whether these cancer cell membrane-covered nanocarriers could cross the blood–brain barrier in vitro. After 8 h, the mixture in the lower chamber was collected to detect the CY5 fluorescence intensity (Figure 3B) and chloride concentration (Figure 3A). The results from the two methods revealed that B16-PAM-SiO<sub>2</sub>, 4T1-PAM-SiO<sub>2</sub>, PAW-PAM-SiO<sub>2</sub> and GI261-PAM-SiO<sub>2</sub> were significantly better able to penetrate the BBB than was PAM-SiO<sub>2</sub>, and the penetration rates were consistent with those of B16-PAM-SiO<sub>2</sub>, GI261-PAM-SiO<sub>2</sub>, RAW-PAM-SiO<sub>2</sub>, 4T1-PAM-SiO<sub>2</sub>, and PAM-SiO<sub>2</sub>.

We expect CMCNPs to inherit most of the interfacial features of the original cell, such as immune escape capabilities. The ability of PAM-SiO<sub>2</sub>, B16-PAM-SiO<sub>2</sub>, 4T1-PAM-SiO<sub>2</sub>, RAW-PAM-SiO<sub>2</sub> and GI261-PAM-SiO<sub>2</sub> to escape phagocytosis by RAW264.7 macrophages in mice was determined by laser confocal microscopy and flow cytometry. The fluorescence of the cells incubated with the membrane-masked nanoparticles (B16-PAM-SiO<sub>2</sub>, 4T1-PAM-SiO<sub>2</sub>, RAW-PAM-SiO<sub>2</sub> and GI261-PAM-

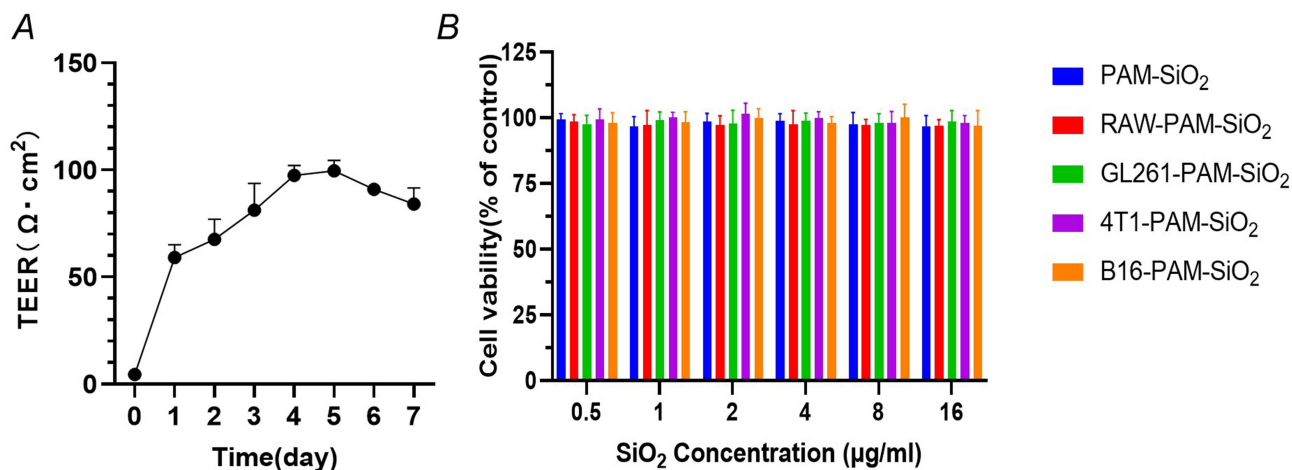


Figure 2 (A) TEER monitoring of the A.hCMEC/D3 monolayer culture model. (B) Cytotoxic effects of different nanoparticles on hCMEC/D3 cells (n=8).

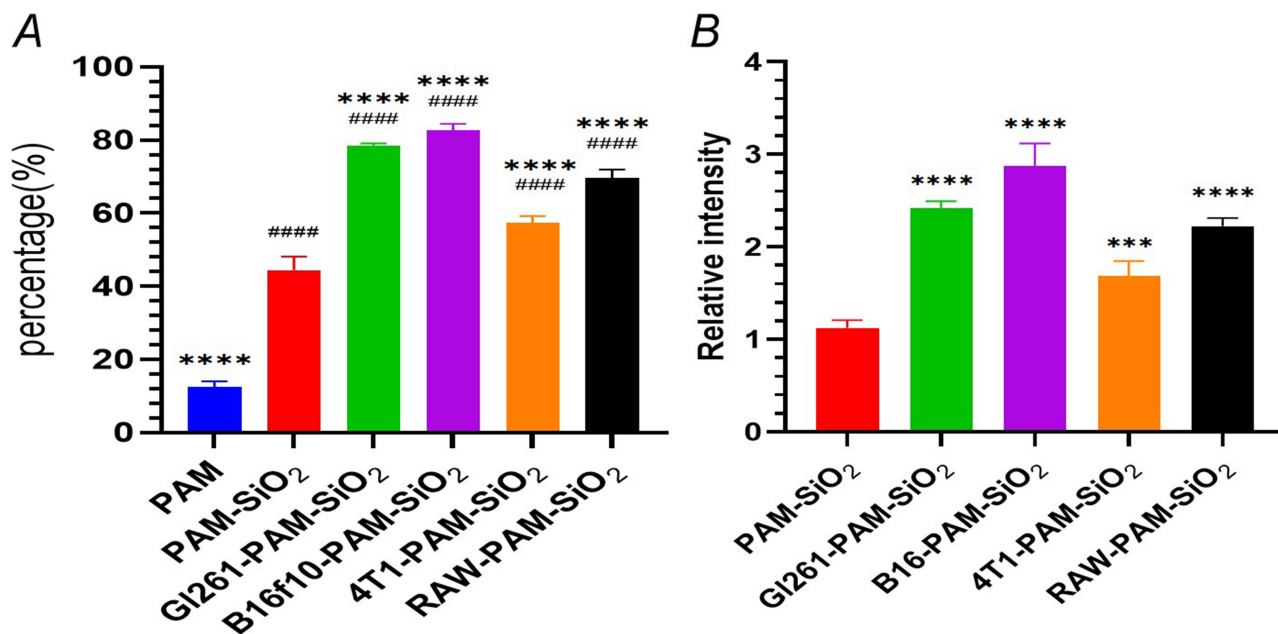


Figure 3 (A) Nanoparticle penetration through the BBB in vitro. Proportion of pralidoxime chloride penetrating the BBB in vitro. (B) The fluorescence intensity of nanosilica spheres penetrating the BBB in vitro (n=3). Compared with the PAM-SiO<sub>2</sub> group, \*\*\*\*P<0.0001 and \*\*\*P<0.001; compared with the PAM group,####P<0.0001.

SiO<sub>2</sub>) was very weak, whereas intense red fluorescence was observed in the cells treated with the uncoated nanoparticles (PAM-SiO<sub>2</sub>) (Figure 4A); the fluorescence of the PAM-SiO<sub>2</sub> nanoparticles was 2.4 times stronger than that of the biomimetic nanoparticles (Figure 4B and C). These results revealed that the immune escape ability of the nanoparticles was significantly improved (p < 0.0001) in the order of GL261-PAM-SiO<sub>2</sub>, B16f10-PAM-SiO<sub>2</sub>, RAW-PAM-SiO<sub>2</sub>, 4T1-PAM-SiO<sub>2</sub>, and PAM-SiO<sub>2</sub>.

### In vivo Studies

The in vitro experiments showed that biomimetic nanoparticles exhibited significant advantages in penetrating the BBB and evading the immune system, with GL261-PAM-SiO<sub>2</sub> and B16-PAM-SiO<sub>2</sub> being the most effective. These two preparations were chosen for further in vivo trials.

First, fluorescence imaging was performed in vivo to detect the distribution of nanoparticles in the body, especially in the mouse brain. PAM-SiO<sub>2</sub>, B16-PAM-SiO<sub>2</sub>, and GL261-PAM-SiO<sub>2</sub> were injected intravenously into healthy mice with

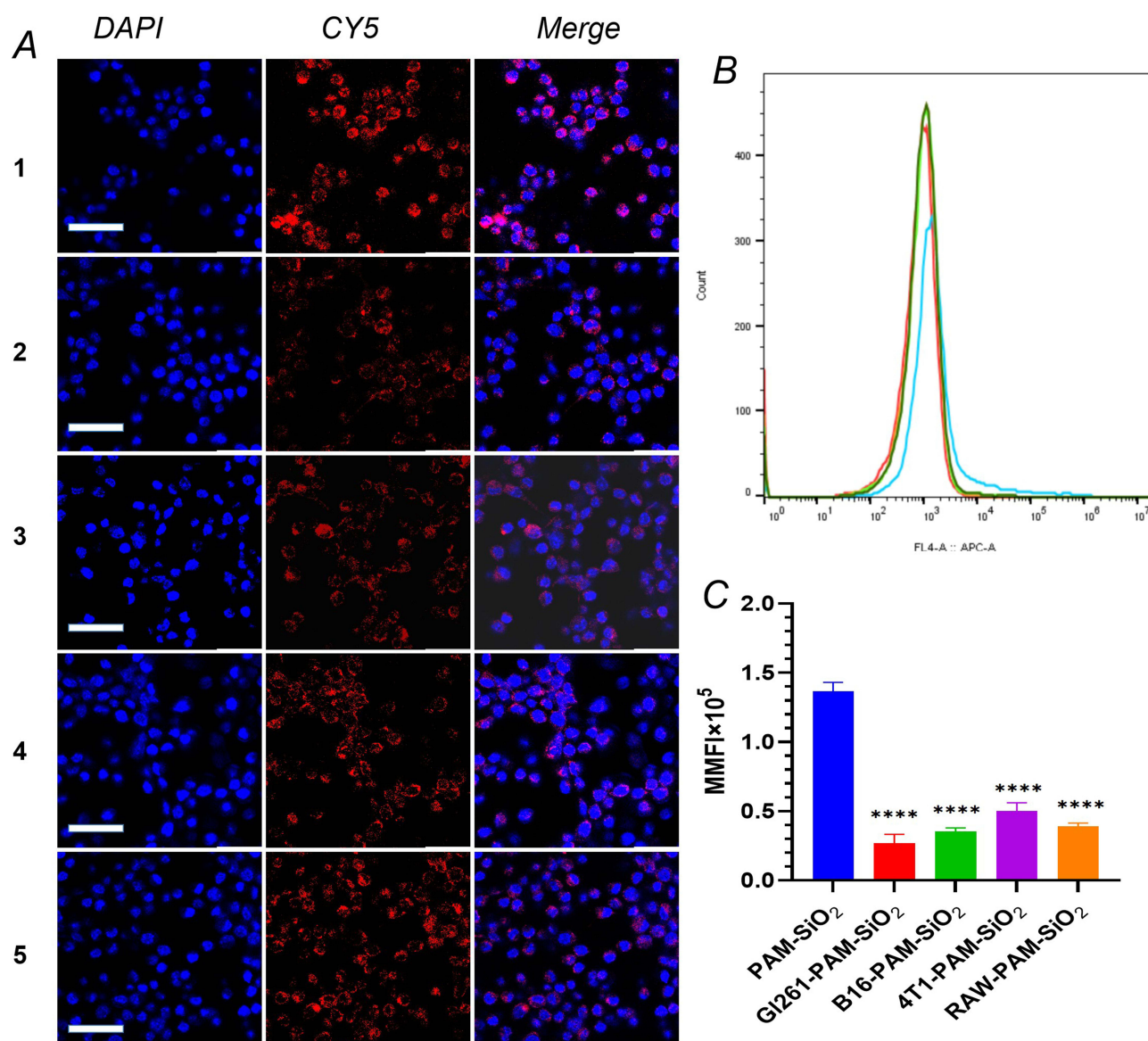


**Figure 4** In vitro immune escape conditions. **(A)** Confocal images of RAW264.7 cells cocultured with 1. PAM-SiO<sub>2</sub>, 2. B16-PAM-SiO<sub>2</sub>, 3. 4T1-PAM-SiO<sub>2</sub>, 4. RAW-PAM-SiO<sub>2</sub>, and 5. GL261-PAM-SiO<sub>2</sub> for 8 hours. SiO<sub>2</sub> content=16 μg/mL. Nuclei were stained with DAPI. Scale bar = 50 μm. **(B)** Flow cytometry analysis of RAW264.7 cells cocultured with B16-PAM-SiO<sub>2</sub> (Orange line), 4T1-PAM-SiO<sub>2</sub> (green line), RAW-PAM-SiO<sub>2</sub> (black line), GL261-PAM-SiO<sub>2</sub> (red line), and PAM-SiO<sub>2</sub> (blue line) for 8 hours. **(C)** Average fluorescence intensity of SiO<sub>2</sub> in RAW264.7 cells treated with different nanoparticles. n=4. Compared with the PAM-SiO<sub>2</sub> group, \*\*\*\*p<0.0001.

an intact BBB. At 2 hours after the injection, particularly at 4 hours, stronger fluorescence signals were observed in the brain regions of the mice injected with B16-PAM-SiO<sub>2</sub> and GL261-PAM-SiO<sub>2</sub> (Figure 5A), indicating that SiO<sub>2</sub> coated with cancer cell membranes could cross the intact BBB and enter the brain. However, no significant accumulation was observed in the brains of the mice injected with uncoated nanoparticles (PAM-SiO<sub>2</sub>). A quantitative analysis using Living Image 4.4 revealed that the fluorescence intensities in the brain regions of the mice injected with B16-PAM-SiO<sub>2</sub> and GL261-PAM-SiO<sub>2</sub> were 3.5 and 2.5 times higher, respectively, than those in the brain regions of the mice injected with PAM-SiO<sub>2</sub> at 4 hours after the injection (Figure 5B). Moreover, fluorescence in the brain tissue at the 24-hour time point was visibly stronger in the mice injected with B16-PAM-SiO<sub>2</sub> and GL261-PAM-SiO<sub>2</sub> than in those injected with PAM-SiO<sub>2</sub> (Figure 6), indicating that silica coated with cell membranes can efficiently enter the BBB and accumulate within the brain.

The live fluorescence results confirmed the ability of the CMCNPs to pass through the BBB. The next step involved injecting CMCNPs into organophosphorus-poisoned mice to assess the ability of the CMCNPs to counteract central

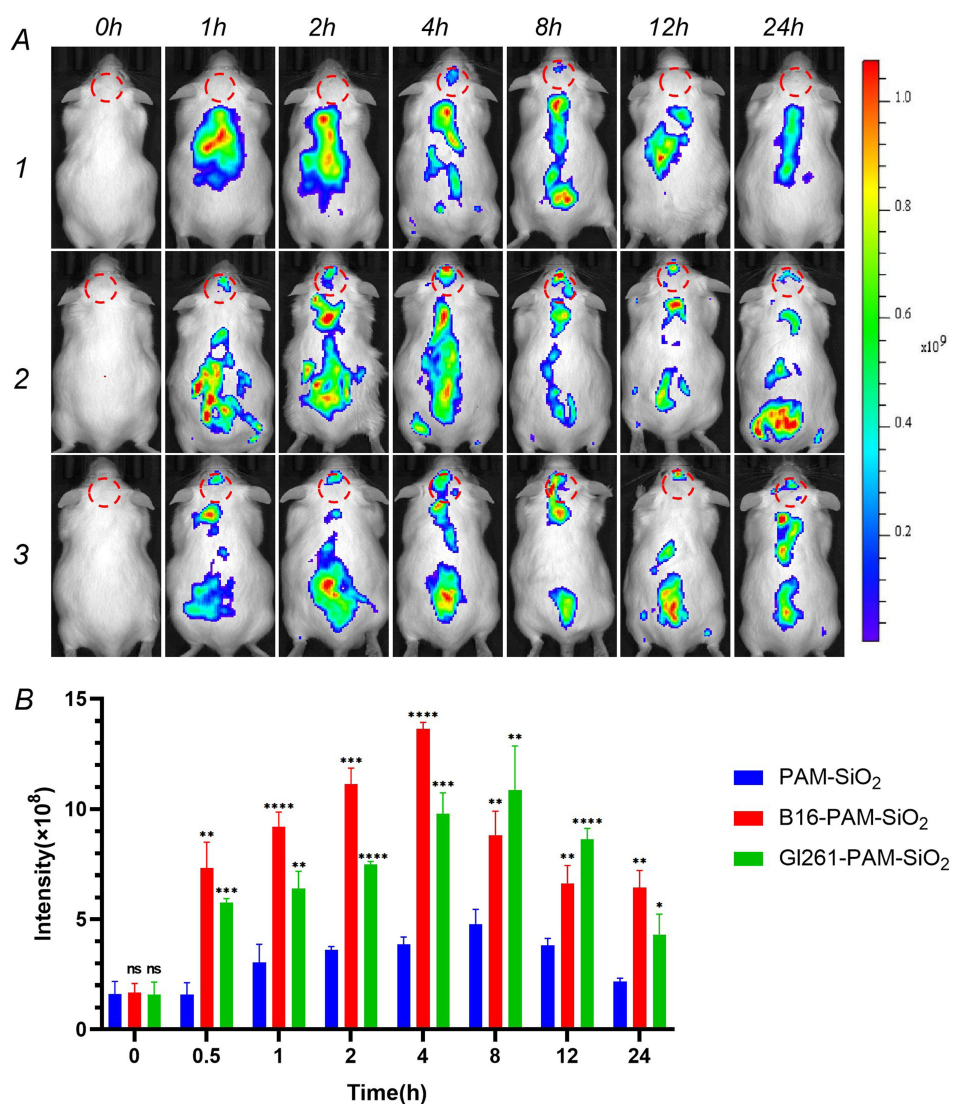


**Figure 5** Live fluorescence imaging. **(A)** Real-time fluorescence imaging of the mice at various time points. 1. PAM-SiO<sub>2</sub>, 2. B16-PAM-SiO<sub>2</sub> and 3. GL261-PAM-SiO<sub>2</sub> **(B)** Corresponding quantitative analysis of fluorescence in the brain. The fluorescence contrast was analyzed using software. The results obtained at all time points were compared with those of the PAM-SiO<sub>2</sub> group. ns: no significant difference; \**p*<0.05; \*\**p*<0.01; \*\*\**p*<0.001; \*\*\*\**p*<0.0001.

organophosphorus poisoning. After the subcutaneous injection of 1.25 g/kg malathion into the mice, saline, PAM, PAM-SiO<sub>2</sub>, B16-PAM-SiO<sub>2</sub>, or GL261-PAM-SiO<sub>2</sub> was injected. The PAM concentrations in the serum and brain homogenate supernatants were measured by high-performance liquid chromatography at 4 h, 12 h, and 24 h, and the serum and brain homogenate supernatants were tested for AChE activity using Ellman’s method. The concentration of chlorpyrifos oxime, AChE activity, and the reactivation rate of AChE in the brains of the mice injected with B16-PAM-SiO<sub>2</sub> and GL261-PAM-SiO<sub>2</sub> were significantly higher than those in the groups administered uncoated PAM-SiO<sub>2</sub> nanoparticles or free PAM (Figure 7A, C and E). In terms of the serum chlorpyrifos oxime concentration, the rate of AChE activity, and the reactivation rate of serum AChE (Figure 7B, D and F), although the serum chlorpyrifos oxime concentration and AChE activity measured at 4 h and 12 h in the mice injected with B16-PAM-SiO<sub>2</sub> and GL261-PAM-SiO<sub>2</sub> were not as good as those in the groups administered uncoated PAM-SiO<sub>2</sub> nanoparticles or free PAM), at 24 h, the serum chlorpyrifos oxime concentrations of the B16-PAM-SiO<sub>2</sub> and GL261-PAM-SiO<sub>2</sub> groups were higher than those in the groups administered uncoated PAM-SiO<sub>2</sub> nanoparticles or free PAM, and the activities of AChE in the groups administered uncoated PAM-SiO<sub>2</sub> nanoparticles or free PAM were not significantly different, indicating that the cell membrane coating effectively prolonged the circulation time of the drug in the body.

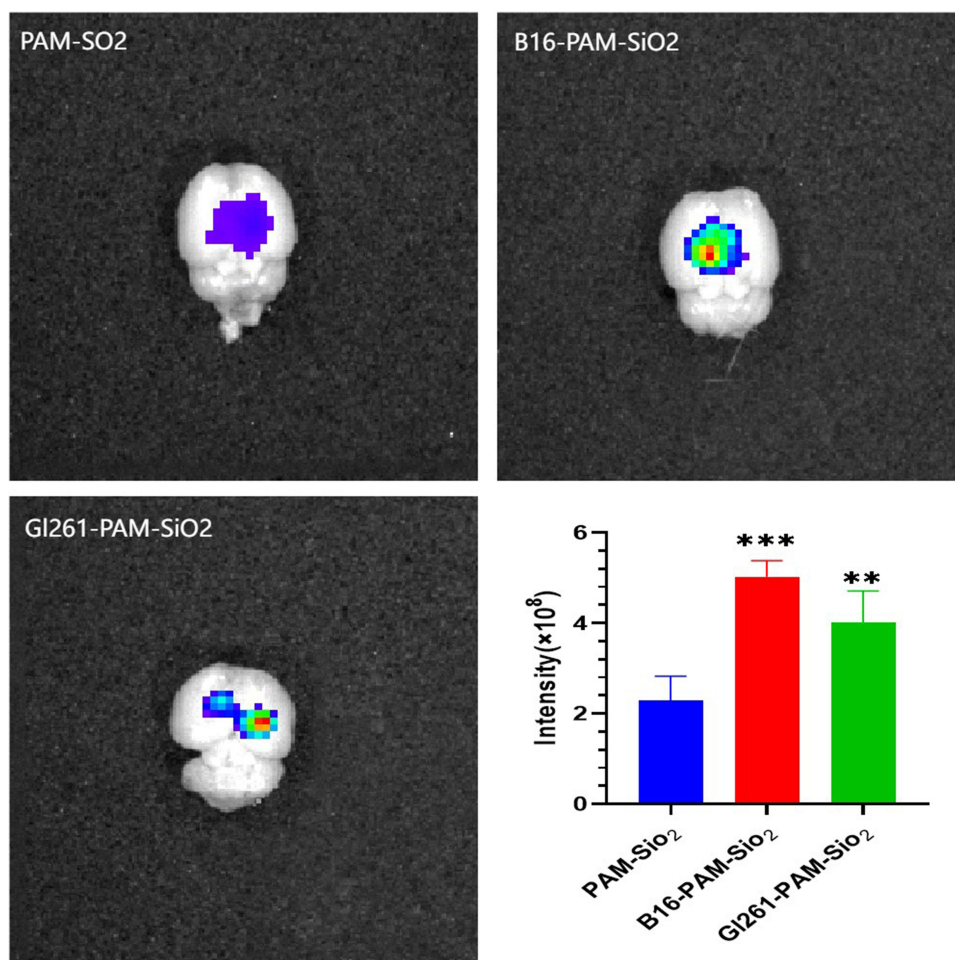


**Figure 6** Fluorescence in the brain tissue at the 24-hour time point. The fluorescence contrast was analyzed using software. The results were compared with those of the PAM-SiO<sub>2</sub> group. \*\* $p < 0.01$ ; \*\*\* $p < 0.001$ .

An analysis of the overall survival rate of the animals was conducted to further clarify the advantages of the membrane-coated nanocarriers in rescuing malathion-poisoned mice. Fifty Kunming mice were randomly divided into 5 groups (10 mice in each group) and subcutaneously injected with 1.5 g/kg malathion. One hour later, the survival of the mice injected via the tail vein with PAM, PAM-SiO<sub>2</sub>, B16-PAM-SiO<sub>2</sub>, GL261-PAM-SiO<sub>2</sub>, saline, or 22.5 mg/kg (1/4LD50) chlorophospidine was recorded at three time points: 4 h, 12 h and 24 h. The survival status of the mice indicated that B16-PAM-SiO<sub>2</sub> and GL261-PAM-SiO<sub>2</sub> were significantly superior to unencapsulated PAM-SiO<sub>2</sub> and free PAM in rescuing the mice from malathion poisoning (Table 2).

## Discussion

Recent strategies for the BBB penetration of pralidoxime have included obtaining compounds with both an excellent reactivation ability and BBB permeability through molecular structural modifications, such as developing prodrugs of pralidoxime such as Pro-PAM,<sup>28</sup> developing monoquatary oximes, and altering the compound structure to a cis-isomer.<sup>29</sup> Further research revealed that the synthesis of the pro-PAM drug is quite difficult and that pro-2-PAM is inherently unstable and prone to oxidation.<sup>28</sup> Although the penetration ability of monoquatary oximes or cis-isomers has improved, their therapeutic efficacy has decreased.<sup>30</sup> This experiment aimed to obtain a drug that can penetrate the BBB while ensuring the efficacy of cholinesterase reactivation; hence, CMCNPs with a core-shell structure were constructed by applying cell membranes to the surface of presynthesized nanoparticles.<sup>17</sup> This study used tumor cell membranes to coat mesoporous silica loaded with PAM to penetrate the BBB and counteract central nervous system organophosphate poisoning. The core nanoparticle used in this experiment was mesoporous silica, which has good

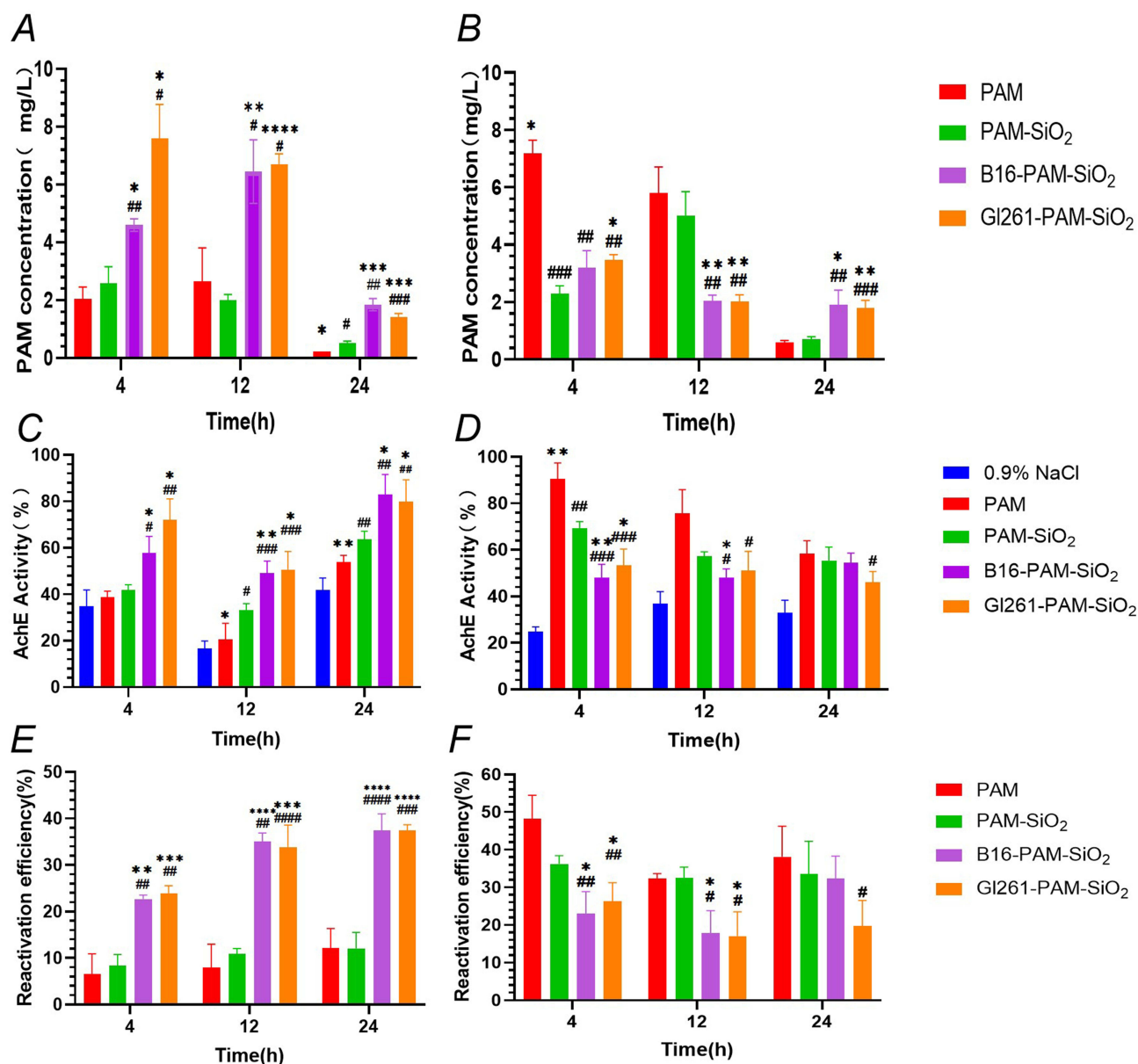


**Figure 7** Pharmacokinetics and pharmacodynamics. Concentrations of pralidoxime chloride in the brain homogenate (A) and serum (B); activities of AChE in brain homogenate (C) and serum (D); reactivation rates of AChE in brain homogenate (E) and serum (F) at different times after the intravenous tail vein injection; n=5 (due to mouse death, the sample size for the 0.9% NaCl group at the 12 h and 24 h time points was 3, and that for the PAM group at 12 h was 4). Compared with the PAM group, #p<0.05, ##p<0.01, ###p<0.001, and ####p<0.0001. Compared with the PAM-SiO<sub>2</sub> group, \*p<0.05, \*\*p<0.01, \*\*\*p<0.001, and \*\*\*\*p<0.0001. No significant difference was detected if not indicated.

biocompatibility and a porous, sponge-like structure that can ensure the adsorption of many drug molecules while maintaining a direct drug release channel to the outside, making it particularly suitable for the treatment of organophosphate poisoning, which requires rapid drug release into the brain.<sup>31,32</sup> Mesoporous silica nanoparticles are recognized for their excellent biocompatibility and high drug-loading capacity. In a subchronic toxicity assessment, mice receiving 50 mg/kg MSNs via intravenous injection twice weekly for 8 weeks presented no adverse effects on body weight, organ indices (liver, spleen, or kidney), or blood biochemistry ( $p > 0.05$  compared with the saline controls).<sup>33</sup> These findings, which are consistent with ISO 10993-11 standards, support the use of silica-based carriers for the targeted delivery of oxime therapeutics (eg, pralidoxime) in organophosphate poisoning models. The cell membranes were selected from tumor cells that often metastasize to the brain, primary brain tumors, and macrophages that perform immune functions. Brain metastasis is a common complication of most tumors, including breast cancer and melanoma, with approximately

**Table 2** Survival Status of the Mice at Various Time Points

Group	n <sup>4</sup> /N	n <sup>12</sup> /N	n <sup>24</sup> /N
0.9% NaCl	8/10	6/10	5/10
PAM	9/10	8/10	7/10
PAM-SiO <sub>2</sub>	9/10	8/10	8/10
GL261-PAM-SiO <sub>2</sub>	10/10	10/10	10/10
B16-PAM-SiO <sub>2</sub>	10/10	9/10	9/10

**Notes:** N represents the total number of mice in the group; n<sup>4</sup> represents the number of surviving mice in the 4-hour group; n<sup>12</sup> represents the number of surviving mice in the 12-hour group; and n<sup>24</sup> represents the number of surviving mice in the 24-hour group.

20% to 30% of malignant tumors able to metastasize to the brain. Therefore, these tumors have the ability to cross the BBB. The adhesion and transendothelial migration of tumor cells to the main components of the blood–brain barrier, brain endothelial cells, are mediated by the interaction of proteins on the tumor cell membrane with adhesion molecules on brain endothelial cells, such as integrins, selectins, and chemokines.<sup>34</sup> Tumor cell membrane proteins exhibit exceptional BBB penetration and immune evasion capabilities, rendering tumor cell membrane-coated NPs more promising than uncoated NPs as therapeutic agents.<sup>35</sup> The superior penetration mechanism of tumor cell membrane-coated nanoparticles across the BBB has not yet been comprehensively elucidated. However, Zou et al proposed that these nanoparticles downregulate the expression of tight junction proteins (ZO-1 and Claudin-5) in endothelial cells, thereby disrupting intercellular tight junctions.<sup>36</sup> Additionally, integrins on the cell membrane may facilitate the adhesion of biomimetic nanoparticles to endothelial cells within the BBB.<sup>34</sup> The immune evasion properties of CMCNPs are closely associated with surface proteins derived from the source tumor cell membrane. For example, CMCNPs retain proteins such as CD47 and CD55, which bind to inhibitory receptors (eg, SIRP $\alpha$  on macrophages), thereby reducing clearance by the reticuloendothelial system and preventing macrophage-mediated attacks.<sup>37</sup> This mechanism is supported by our flow cytometry data, which revealed a 2.4-fold reduction in macrophage uptake of the CMCNPs and subsequent prolongation of the systemic circulation time. Researchers have inferred that the tumor cell membrane plays a key role in brain metastasis; hence, we selected tumor cells that often metastasize to the brain, such as breast cancer and melanoma cells. In addition, considering that glioma cells originate from the brain and that macrophages cross the BBB while performing immune functions, this study included two other cell types, namely, mouse glioma cells and mouse monocyte macrophage leukemia cells, for membrane extraction, with the hope that nanoparticles coated with these membranes would inherit these characteristics. The four types of membrane-coated nanoparticles were subjected to the same experimental conditions for in vitro control screen, and according to the results presented in vitro model testing, B16-PAM-SiO<sub>2</sub> showed an advantage in its ability to cross the BBB, and GL261-PAM-SiO<sub>2</sub> showed an advantage in avoiding immune cell phagocytosis; hence, B16-PAM-SiO<sub>2</sub> and GL261-PAM-SiO<sub>2</sub> were chosen for subsequent pharmacodynamic and pharmacokinetic experiments.

Malathion, a broad-spectrum organophosphorus pesticide, is widely used in agricultural production, leading to frequent incidents of organophosphorus poisoning.<sup>38,39</sup> Therefore, this study established an animal model of organophosphorus poisoning by subcutaneously injecting mice with 1.25 g/kg malathion. The experimental treatments included an intravenous tail injection of PAM, PAM-SiO<sub>2</sub>, B16-PAM-SiO<sub>2</sub>, or GL261-PAM-SiO<sub>2</sub> containing 22.5 mg/kg (1/4LD50) PAM. The AChE reactivation rate was measured, and the survival status of the mice was observed. According to the results of the AChE activity determination for the treatment of central nervous system organophosphorus poisoning, the groups treated with the cell membrane-coated B16-PAM-SiO<sub>2</sub> and GL261-PAM-SiO<sub>2</sub> nanoparticles presented better AChE reactivation than did the groups that received uncoated PAM-SiO<sub>2</sub> or free PAM. Owing to the ability of the nanoparticles to enter the CNS and achieve sustained release, the peripheral blood systemic concentrations of PAM in the groups receiving cell membrane-coated B16-PAM-SiO<sub>2</sub> and GL261-PAM-SiO<sub>2</sub> were not as high as those in the groups receiving uncoated PAM-SiO<sub>2</sub> and free PAM at the first time point (12 hours), but at the 24-hour time point, the CMCNPs had longer circulation times. According to the overall animal survival rates, the cell membrane-coated B16-

PAM-SiO<sub>2</sub> and GL261-PAM-SiO<sub>2</sub> nanoparticles clearly presented advantages. We believe that the cell membrane-coated B16-PAM-SiO<sub>2</sub> and GL261-PAM-SiO<sub>2</sub> nanoparticles inherited the original biological functions of the tumor cell membrane, helping PAM penetrate the BBB to mitigate central malathion poisoning. Given the disadvantages of CMCNPs, namely, low PAM concentrations in the peripheral blood circulation and low AChE reactivation rates in the initial period, we believe that central and peripheral organophosphorus poisoning can be resolved by administering both free PAM and cell membrane-coated drug-loaded nanoparticles. This study utilized CMCNPs to load and deliver organophosphorus antidotes, increasing the penetration of the antidotes through the BBB and transporting the target drugs to the brain for release, verifying that CMCNPs have potential as a strategy for delivering organophosphorus antidotes.

Although this study verified the various advantages of CMCNPs in delivering drugs into the CNS, some limitations to their widespread application also exist, such as the difficulty of extracting large quantities of cell membranes and the tendency for cell membranes to degrade and surface proteins to become inactive during storage, which can affect the performance of CMCNPs. Challenges in controlling the uniformity and consistency of cell membranes during the preparation of CMCNPs also exist. Furthermore, as biological products, CMCNPs must be comprehensively evaluated by regulatory agencies such as the FDA/EMA in accordance with biologic product standards prior to their clinical application.<sup>40</sup> These problems need to be addressed in further research.

## Conclusions

This study developed a bioinspired nanoparticle platform that successfully overcomes the critical challenge of BBB penetration in the treatment of organophosphate poisoning. By combining tumor cell membrane coatings (B16F10, 4T1, GL261, and RAW264.7 cell membranes) with PAM-loaded mesoporous silica nanoparticles, we achieved three key breakthroughs: (1) The successful construction of four types of CMCNPs loaded with pralidoxime chloride—B16-PAM-SiO<sub>2</sub>, 4T1-PAM-SiO<sub>2</sub>, RAW-PAM-SiO<sub>2</sub>, and GL261-PAM-SiO<sub>2</sub>; (2) In tests of the in vitro model, CMCNPs demonstrated an enhanced immune evasion ability and BBB penetration ability; (3) CMCNPs had advantages in treating CNS organophosphate poisoning in mice, such as an increased delivery of PAM to the CNS that significantly increased brain cholinesterase activity in poisoned mice, a prolonged systemic circulation time of PAM and an improved survival rate in mice. Compared with traditional therapeutic approaches, this CMCNPs platform significantly increases the efficiency of PAM delivery to the CNS, with the potential to overcome the clinical limitations associated with current cholinesterase reactivators.

Our research provides a potentially effective strategy for treating CNS symptoms caused by organophosphate poisoning.

## Ethical Approval and Consent to Participate

All the animal experiments were approved by the Ethics Committee of the State Key Laboratory of NBC Protection for Civilian (#LAE-2024-04-007), and the animal care and experimentation procedures followed the Guide for the Care and Use of Laboratory Animals published by the National Institutes of Health (NIH publication no. 85–23, revised 1996).

## Acknowledgments

The authors thank the anonymous reviewers for their insightful comments.

## Disclosure

The authors declare that they have no known competing financial interests or personal relationships that could have appeared to influence the work reported in this paper.

## References

1. Xu W, Zhao S, Zhang W, Wu H, Guang C, Mu W. Recent advances and future prospective of organophosphorus-degrading enzymes: identification, modification, and application. *Crit Rev Biotechnol.* 2021;41(7):1096–1113. doi:10.1080/07388551.2021.1898331

2. Singh BK. Organophosphorus-degrading bacteria: ecology and industrial applications. *Nat Rev Microbiol.* 2008;7(2):156–164. doi:10.1038/nrmicro2050
3. Jeyaratnam J. Acute pesticide poisoning: a major global health problem. *World Health Stat.* 1990;43(3):139–144.
4. Prchalova E, Kohoutova Z, Knittelova K, Malinak D, Musilek K. Strategies for enhanced bioavailability of oxime reactivators in the central nervous system. *Arch Toxicol.* 2023;97(11):2839–2860. doi:10.1007/s00204-023-03587-0
5. de Koning MC, van Grol M, Noort D. Peripheral site ligand conjugation to a non-quaternary oxime enhances reactivation of nerve agent-inhibited human acetylcholinesterase. *Toxicol Lett.* 2011;206(1):54–59. doi:10.1016/j.toxlet.2011.04.004
6. Faiz Norraahim MN, Idayu Abdul Razak MA, Ahmad Shah NA, et al. Recent developments on oximes to improve the blood brain barrier penetration for the treatment of organophosphorus poisoning: a review. *RSC Adv.* 2020;10(8):4465–4489. doi:10.1039/c9ra08599h
7. Bierwisch A, Wille T, Thiermann H, Worek F. Kinetic analysis of interactions of amodiaquine with human cholinesterases and organophosphorus compounds. *Toxicol Lett.* 2016;246:49–56. doi:10.1016/j.toxlet.2016.02.004
8. Mohammed PN, Hussien NH, Hasan AH, et al. A review on the role of nanoparticles for targeted brain drug delivery: synthesis, characterization, and applications. *Excli J.* 2025;24:34–59. doi:10.17179/excli2024-7163
9. Tsou YH, Zhang XQ, Zhu H, Syed S, Xu X. Drug delivery to the brain across the blood–brain barrier using nanomaterials. *Small.* 2017;13(43). doi:10.1002/smll.201701921
10. Hussien NHA, Qadir SH, Rahman HS, Hamalaw YY, Kareem PSS, Hamza BA. Long-term toxicity of fluoroquinolones: a comprehensive review. *Drug Chem Toxicol.* 2024;47(5):795–806. doi:10.1080/01480545.2023.2240036
11. Hussien NH, Hasan AH, FaqiKhedr YM, Bogoyavlenskiy A, Bhat AR, Jamalis J. Carbon dot based carbon nanoparticles as potent antimicrobial, antiviral, and anticancer agents. *ACS Omega.* 2024;9(9):9849–9864. doi:10.1021/acsomega.3c05537
12. Yan Z, Wang D, Gao Y. Nanomaterials for the treatment of bacterial infection by photothermal/photodynamic synergism. *Front Bioeng Biotechnol.* 2023;11:1192960. doi:10.3389/fbioe.2023.1192960
13. Wu S, Li A, Zhao X, et al. Silica-coated gold–silver nanocages as photothermal antibacterial agents for combined anti-infective therapy. *ACS Appl Mater Interfaces.* 2019;11(19):17177–17183. doi:10.1021/acsami.9b01149
14. Hussien NH, Hasan AH, Muhammed GO, et al. Anthracycline in medicinal chemistry: mechanism of cardiotoxicity, preventive and treatment strategies. *Curr Org Chem.* 2023;27(4):363–377. doi:10.2174/1385272827666230423144150
15. Yang J, Fan L, Wang F, et al. Rapid-releasing of HI-6 via brain-targeted mesoporous silica nanoparticles for nerve agent detoxification. *Nanoscale.* 2016;8(18):9537–9547. doi:10.1039/c5nr06658a
16. Xie J, Shen Z, Anraku Y, Kataoka K, Chen X. Nanomaterial-based blood-brain-barrier (BBB) crossing strategies. *Biomaterials.* 2019;224. doi:10.1016/j.biomaterials.2019.119491
17. Fang RH, Kroll AV, Gao W, Zhang L. Cell MEMBRANE COATING NANOTEchnology. *Adv Mater.* 2018;30(23). doi:10.1002/adma.201706759
18. Anchordoquy TJ, Barenholz Y, Boraschi D, et al. Mechanisms and barriers in cancer nanomedicine: addressing challenges, looking for solutions. *ACS Nano.* 2017;11(1):12–18. doi:10.1021/acsnano.6b08244
19. Wang C, Wu B, Wu Y, Song X, Zhang S, Liu Z. Camouflaging nanoparticles with brain metastatic tumor cell membranes: a new strategy to traverse blood–brain barrier for imaging and therapy of brain tumors. *Adv Funct Mater.* 2020;30(14). doi:10.1002/adfm.201909369
20. Han Y, Gao C, Wang H, et al. Macrophage membrane-coated nanocarriers co-modified by RVG29 and TPP improve brain neuronal mitochondria-targeting and therapeutic efficacy in Alzheimer’s disease mice. *Bioact Mater.* 2021;6(2):529–542. doi:10.1016/j.bioactmat.2020.08.017
21. Liu H, Han Y, Wang T, et al. Targeting microglia for therapy of parkinson’s disease by using biomimetic ultrasmall nanoparticles. *J Am Chem Soc.* 2020;142(52):21730–21742. doi:10.1021/jacs.0c09390
22. Qiu S, Zhu F, Tong L. Application of targeted drug delivery by cell membrane-based biomimetic nanoparticles for inflammatory diseases and cancers. *Eur J Med Res.* 2024;29(1):523. doi:10.1186/s40001-024-02124-8
23. Ogunshola OO. In vitro modeling of the blood-brain barrier: simplicity versus complexity. *Curr Pharm Des.* 2011;17(26):2755–2761. doi:10.2174/138161211797440159
24. Siflinger-Birnboim A, Del Vecchio PJ, Cooper JA, Blumenstock FA, Shepard JM, Malik AB. Molecular sieving characteristics of the cultured endothelial monolayer. *J Cell Physiol.* 1987;132(1):111–117. doi:10.1002/jcp.1041320115
25. Weksler B, Romero IA, Couraud PO. The hCMEC/D3 cell line as a model of the human blood brain barrier. *Fluids Barriers CNS.* 2013;10(1):16. doi:10.1186/2045-8118-10-16
26. Ragnai MN, Brown M, Ye D, et al. Internal benchmarking of a human blood–brain barrier cell model for screening of nanoparticle uptake and transcytosis. *Eur J Pharm Biopharm.* 2011;77(3):360–367. doi:10.1016/j.ejpb.2010.12.024
27. Deli MA, Abrahám CS, Kataoka Y, Niwa M. Permeability studies on in vitro blood-brain barrier models: physiology, pathology, and pharmacology. *Cell Mol Neurobiol.* 2005;25(1):59–127. doi:10.1007/s10571-004-1377-8
28. Kalisiak J, Ralph EC, Zhang J, Cashman JR. Amidine–oximes: reactivators for organophosphate exposure. *J Med Chem.* 2011;54(9):3319–3330. doi:10.1021/jm200054r
29. Karasova JZ, Zemek F, Bajgar J, et al. Partition of bispyridinium oximes (trimedoxime and K074) administered in therapeutic doses into different parts of the rat brain. *J Pharmaceut Biomed Anal.* 2011;54(5):1082–1087. doi:10.1016/j.jpba.2010.11.024
30. Soukup O, Korabecny J, Malinak D, et al. In vitro and in silico evaluation of non-quaternary reactivators of ache as antidotes of organophosphorus poisoning - a new hope or a blind alley? *Med Chem.* 2018;14(3):281–292. doi:10.2174/1573406414666180112105657
31. Vyas J, Singh S, Shah I, Prajapati BG. Potential applications and additive manufacturing technology-based considerations of mesoporous silica: a review. *AAPS Pharm Sci Tech.* 2023;25(1):6. doi:10.1208/s12249-023-02720-7
32. Li Z, Zhang Y, Feng N. Mesoporous silica nanoparticles: synthesis, classification, drug loading, pharmacokinetics, biocompatibility, and application in drug delivery. *Expert Opin Drug Deliv Mar.* 2019;16(3):219–237. doi:10.1080/17425247.2019.1575806
33. Lu J, Liong M, Li Z, Zink JI, Tamanoi F. Biocompatibility, biodistribution, and drug-delivery efficiency of mesoporous silica nanoparticles for cancer therapy in animals. *Small.* 2010;6(16):1794–1805. doi:10.1002/smll.201000538
34. Preusser M, Capper D, Ilhan-Mutlu A, et al. Brain metastases: pathobiology and emerging targeted therapies. *Acta Neuropathol.* 2012;123(2):205–222. doi:10.1007/s00401-011-0933-9
35. Liu Z, Wang F, Liu X, et al. Cell membrane-camouflaged liposomes for tumor cell-selective glycans engineering and imaging in vivo. *Proc Natl Acad Sci U S A.* 2021;118(30). doi:10.1073/pnas.2022769118

36. Zou Y, Wang Y, Xu S, et al. Brain co-delivery of temozolomide and cisplatin for combinatorial glioblastoma chemotherapy. *Adv Mater.* 2022;34(33):e2203958. doi:10.1002/adma.202203958
37. Murata Y, Saito Y, Kotani T, Matozaki T. CD47-signal regulatory protein  $\alpha$  signaling system and its application to cancer immunotherapy. *Cancer Sci.* 2018;109(8):2349–2357. doi:10.1111/cas.13663
38. Tchounwou PB, Patlolla AK, Yedjou CG, Moore PD. Environmental exposure and health effects associated with malathion toxicity. *Toxicity Hazard Agrochem.* 2015;71:1.
39. Elmorsy E, Al-Ghafari A, Al Doghaither H, Salama M, Carter WG. An investigation of the neurotoxic effects of malathion, chlorpyrifos, and paraquat to different brain regions. *Brain Sci.* 2022;12(8):975. doi:10.3390/brainsci12080975
40. Fang RH, Gao W, Zhang L. Targeting drugs to tumours using cell membrane-coated nanoparticles. *Nat Rev Clin Oncol.* 2023;20(1):33–48. doi:10.1038/s41571-022-00699-x

International Journal of Nanomedicine

Publish your work in this journal

The International Journal of Nanomedicine is an international, peer-reviewed journal focusing on the application of nanotechnology in diagnostics, therapeutics, and drug delivery systems throughout the biomedical field. This journal is indexed on PubMed Central, MedLine, CAS, SciSearch<sup>®</sup>, Current Contents<sup>®</sup>/Clinical Medicine, Journal Citation Reports/Science Edition, EMBase, Scopus and the Elsevier Bibliographic databases. The manuscript management system is completely online and includes a very quick and fair peer-review system, which is all easy to use. Visit <http://www.dovepress.com/testimonials.php> to read real quotes from published authors.

Submit your manuscript here: <https://www.dovepress.com/international-journal-of-nanomedicine-journal>

**Dovepress**  
Taylor & Francis Group